Preprint typeset in JINST style - HYPER VERSION

CALICE Analysis Note CAN-043
April 22, 2013

The Time Structure of Hadronic Showers in Tungsten with FastRPC

The CALICE Collaboration*

This note contains preliminary CALICE results, and is for the use of members of the CALICE Collaboration and others to whom permission has been given.*t*

ABSTRACT: We present results on the time structure of hadronic showers in tungsten measured with the FastRPC setup installed behind the CALICE WDHCAL. These results are compared to the measurements taken with the T3B experiment.

*Corresponding authors: Frank Simon (fsimon@mpp.mpg.de), Christian Soldner (soldner@mpp.mpg.de), Marco Szalay (mszalay@mpp.mpg.de), Lars Weuste (weuste@mpp.mpg.de)

Contents

1. Introduction

Understanding the time structure of a hadronic shower is a key aspect to investigate the achievable time resolution for hadronic calorimetry, especially when dealing with the high collision rates, up to 2 GHz, planned at colliders such as CLIC [1]. A previous experiment, T3B [2], based on scintillator tiles coupled to SiPMs, already provided high-precision timing measurements for the CALICE WAHCAL tungsten prototype as well as the SDHCAL steel prototype and compared the results with GEANT4 simulations. The aim of the FastRPC setup is to perform a similar sub-ns precision measurement of the time development of hadronic showers in the CALICE digital tungsten HCAL (WDHCAL) prototype using a glass Resistive Plate Chamber (RPC) as active medium instead of plastic scintillators. Comparing the results of the two experiments, based on completely different detection mechanisms, provides the possibility to study differences in the observed time structure related to different sensitivities of the two detection media to sub-components of hadronic showers. This improves the understanding of the underlying shower physics while avoiding possible misinterpretations caused by peculiarities of a single detector system.

The FastRPC data presented here were recorded in Spring 2012 with the WDHCAL prototype at the CERN SPS in the H8 beam line, with high statistics data sets taken at energies of 80 GeV and 180 GeV.

2. Experimental Setup

For the data taking, the FastRPC detector was installed behind the 38 absorber layers of the WDHCAL prototype [3], at a depth of approximately 5 λ_I.

The setup consists of a glass RPC of the same type as those used for the DHCAL prototype, which was provided by the Argonne group. The RPC was operated with a gas mixture of 94.5%

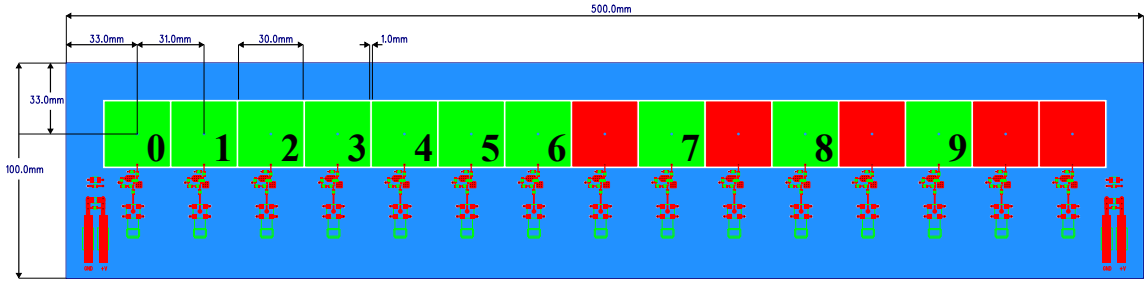

Figure 1: Layout of the FastRPC PCB and readout pads. The nominal beam axis intersects the center of pad 0. The pads marked in red are not read out.

R134A, 5% C_4H_{10} and 0.5% SF_6 and at a voltage of 6.3 kV, identical to the detectors in the WDHCAL.

The readout of the RPC is performed using the data acquisition system developed for T3B. To provide the best basis for a comparison, the same readout granularity is also used for FastRPC. Coupled to the RPC layer, a PCB with fifteen 3×3 cm^2 pads and as many BGA614 preamplifiers sense the charges produced by ionization in the gaseous volume of the RPC and routes the analog signal to USB oscilloscopes[1] capable of sampling it at a frequency of 1.25 GHz with an 8-bit vertical range. The oscilloscopes are externally triggered via a scintillator coincidence, placed before the WDHCAL, that starts the data acquisition of the FastRPC readout. The long sampling window of 2.4 µs allows to study the full time evolution of hadronic showers, including very late components. The readout pads are arranged in a row that extends from the nominal center of the particle beam towards the outer part of the detector to provide a full radial sampling of the hadronic shower. The geometry of the readout structure is shown in figure 1.

Because of a hardware problem with one of the readout oscilloscopes which developed during the data taking period, some of the readout pads (marked in red in figure 1) were disconnected during the data taking and are neglected during the analysis. The channel numbering in the figure is coherent with the numbering scheme used for the results in section 4.

In addition to the readout channels, two additional channels of the data acquisition system were dedicated to monitoring the scintillator coincidence and to the WDHCAL trigger status. This enables double particle events in which the coincidence triggers twice within the 2.4 µs sampling window, to be rejected, and allows for offline data synchronization with the WDHCAL in the future.

FastRPC is triggered by the coincidence of two 10×10 cm^2 scintillators for hadron and muon runs. While the beam spot is substantially smaller than the trigger area for high-energy hadrons, the area covered by muons without substantial multiple scattering is defined by the trigger. The trigger jitter is on the level of 500 ps to 700 ps, with an overall jitter of the time reconstructed for muons, which includes the RPC response, of around 750 ps.

3. Data Analysis

As we will see in section 4, the number of hits in the detector that contributes to the late time

[1] PicoTech PicoScope® 6403 (http://www.picotech.com/)

components of a hadronic shower is up to 10^6 times smaller than the instantaneous components of the shower. Therefore it is crucial to implement a reliable calibration and analysis work-flow capable of rejecting noise artefacts that mimic real signal events with high efficiency.

For this purpose a software filter was developed and successively benchmarked with muon run data. The filter works as follows:

- a 10 mV threshold cut is applied on the raw waveforms recorded by the oscilloscopes to search for candidates for the leading edge of a signal. The time-stamp of every bin where the recorded waveform rises above the threshold is tagged as a possible *time of first hit* candidate.

- a check on the slope of the rising edge of the signal is made in the vicinity of the trigger candidate. At least one of the two bins directly adjacent to the triggered one is required to differ from this by more than 5 mV, otherwise the trigger is rejected. This is done to eliminate low-frequency pick-up noise, with slower rise times, coming from the electronics.

- the ROOT TSpectrum class is used to search for a peak in the waveform within 6 ns after every trigger candidate. If a peak is found, then the trigger candidate gets validated and it is saved for later analysis, otherwise it is rejected, since noise usually shows smoother and broader patterns that do not trigger the peak finder. In muon runs, 20% to 25% of all triggered events have an identified peak, which is consistent with the geometrical coverage of FastRPC compared to the trigger scintillators.

- to reject RPC afterpulsing, such as the examples shown in figure 2, an additional filter step is needed. While for an event like the one shown in figure 2 (*left*), the appropriate rising edge is still correctly identified, an event such as the one in figure 2 (*right*) would lead to a mistag of the time position of the rising edge of the signal by several ns. To prevent this, an additional time window of 15 ns, that is approximately twice the distance between two peaks of an afterpulsing event, before the trigger candidate bin is examined. If a peak is found in this region, the trigger is rejected. The fraction of events that show secondary peaks is on the percent level.

The validity and the performance of the filter chain is studied with muon events. Since these particles interact electromagnetically, their energy deposition in the active layer is instantaneous without any late components. Therefore the time distribution of all triggered muon hits should form a Gaussian peak, whose variance is given by a convolution of the trigger jitter, the jitters and resolutions of the oscilloscopes and the intrinsic time resolution of the RPC. Depending on the level of sophistication of the filters used, this distribution can however also contain hits that are far away from the Gaussian peak. This is illustrated in figure 3 (*left*), which shows an example where only the first filter step has been applied. The hits outside of the expected window originate from various sources, such as RPC afterpulsing, resulting in a secondary peak about 8 ns after the primary one, and common noise pickup possibly due to signal reflections, which generates the events observed at times around 60 ns. Figure 3 (*right*) shows the result of the full filtering chain, where most of the non-signal hits are rejected, with a small contribution form non-rejected afterpulsing on the level of 10^{-4} remaining.

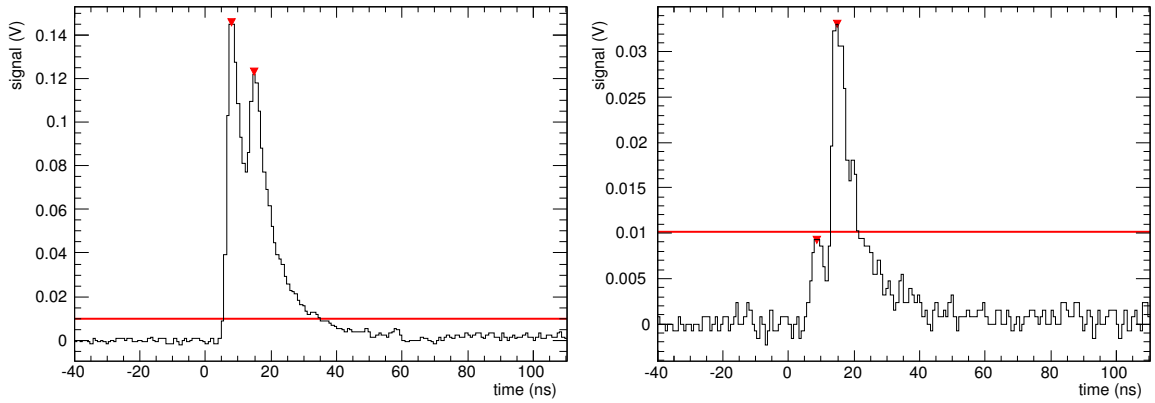

Figure 2: Example of afterpulsing events. In these events a photon, produced in the excitation process, is not absorbed by the quenching gas mixture and starts a secondary shower (the 2nd peak) by extracting an electron at the cathode. The time interval between the consecutive peaks is a rather constant signature, proportional to the drift coefficient of the electrons in the gas and to the thickness of the gaseous layer. The occurrence of the afterpulse would lead to a fake late hit in the example shown on the right, since the first original pulse is below the simple 10 mV threshold.

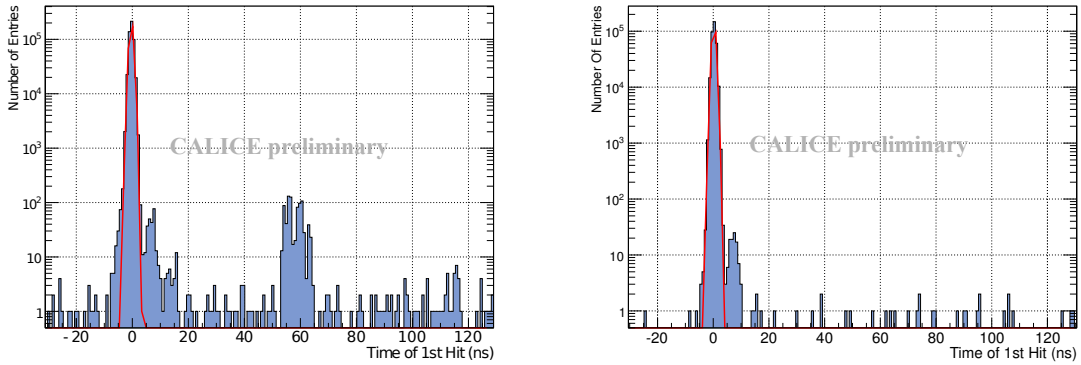

Figure 3: Time distribution of the energy deposition for muons, obtained applying only the first step of the filter chain, a 10 mV threshold cut, on the left and with the entire filter chain on the right. The Gaussian fit in red defines the peak where muons should deposit energy, outside of it are the entries from noise artifacts or streamers that were not properly filtered.

Using muons it is possible to measure the sample purity after a filter is applied, simply by calculating the signal-to-noise ratio between the number of events that are within the Gaussian and those outside. For the entire filter chain described above, using the full 2.4 μs time window, this value is 0.996, showing that noise hits are rejected with high efficiency. A more in-depth explanation of the filter procedure can be found in [4].

4. Results

The FastRPC results presented here use a data set of more than 2.2 million π^+ events at 180 GeV,

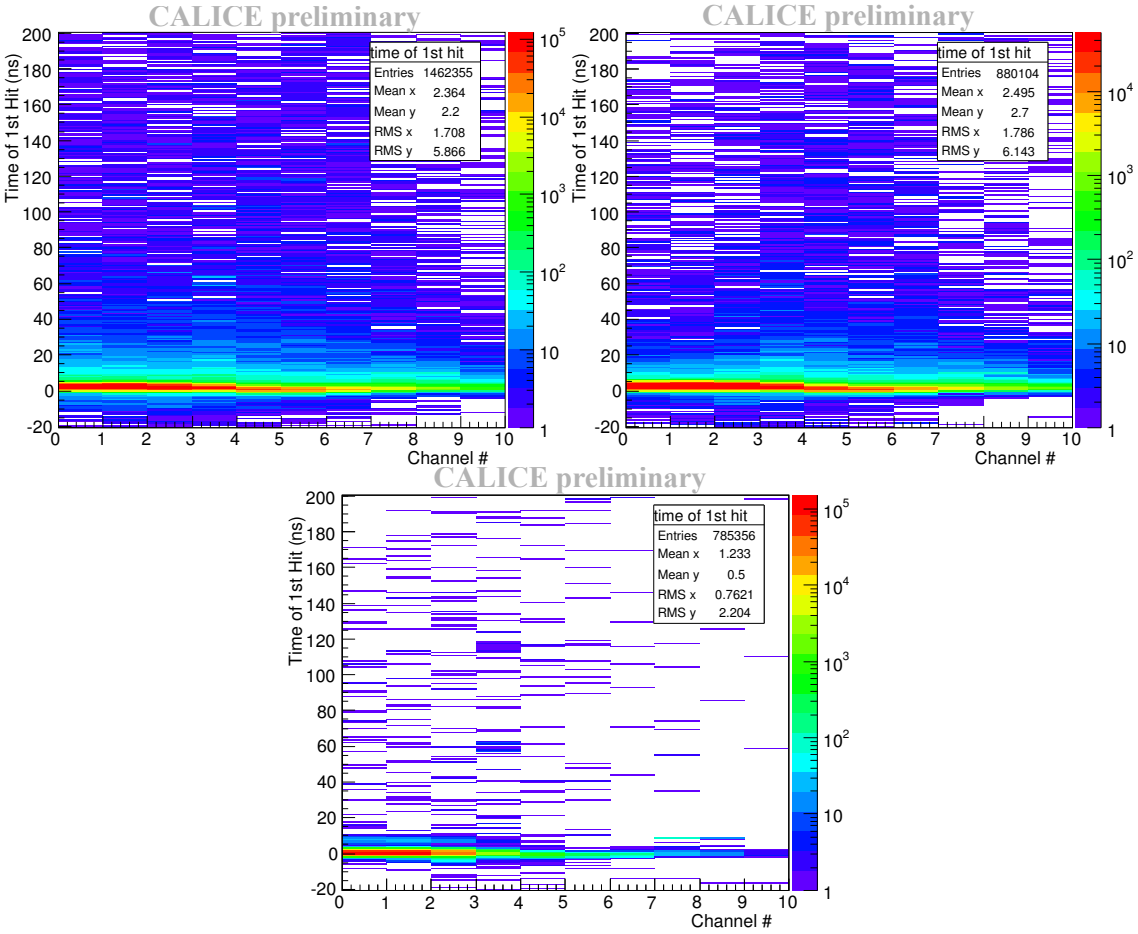

Figure 4: Hits in FastRPC as a function of readout channel and hit time. For each triggered event, only the first hit in each cell is taken into consideration. Upper row: Distributions for 80 GeV $\pi^{\pm}$ (*left*) and 180 GeV π^{+}(*right*). Lower row: Reference distribution for 180 GeV muons. Pion runs exhibit late energy depositions in the FastRPC layer.

2.6 million $\pi^{\pm}$ events at 80 GeV as well as 3 million muon events for reference.

Figure 4 shows the distribution of the time of first hit in the FastRPC layer as a function of the readout channel for 80 and 180 GeV pions as well as the reference distribution for muons. These distributions form the basis of all following analysis, which studies their different projections. From figure 4 it is already apparent that hadronic showers exhibit substantial late contributions in comparison to muons. The time t = 0 is determined for each data set individually by determining the position of the maximum of the prompt signal peak. The uncertainty of this procedure is estimated to be around 200 ps [2].

Time Of First Hit

By projecting the distribution shown in figure 4, onto the time axis, the time distribution of energy deposition in tungsten, shown in figure 5 a), is obtained. Figure 5 b) shows the same distribution, displaying the full 2.4 μs sampling window with the exception of the first 8 ns in a double logarithmic plot. Since the contributions of 80 and 180 GeV pions overlap completely, from these two

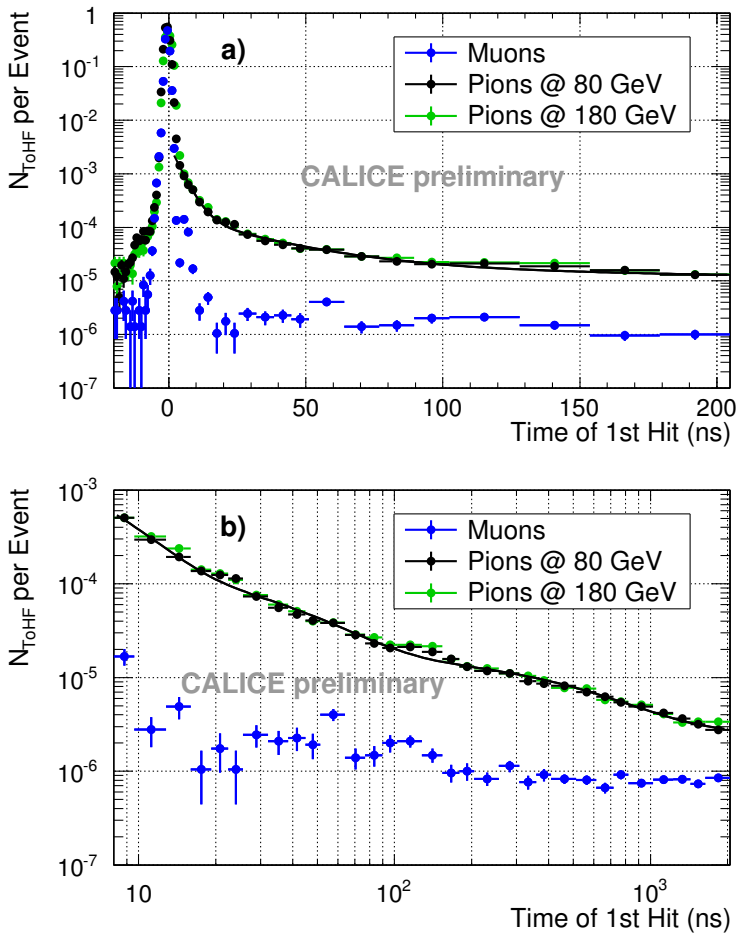

Figure 5: Time distribution of first hits in the FastRPC detector in the [-20, 200] ns region (a) and [8, 2400] ns (b), normalized to the number of events with at least one hit in the FastRPC detector.

figures it looks like the time structure of the late energy deposition does not depend on the particles' energy.

In the distribution, three different time components can be distinguished: (a) a short one (≈[0, 10] ns), coming from instantaneous energy depositions of relativistic particles and the corresponding detector response, (b) an intermediate component (≈[10, 100] ns) primarily due to neutron elastic scattering on the hydrogen nuclei of the active layer and (c) a late time component (≈[100, 1000+] ns) coming from slower nuclear processes such as de-excitation following neutron capture in the absorber.

To extract the separate time constants, a sum of three exponential functions plus a constant term to account for the random noise pedestal and for even longer time components is fitted to the tail of the time distribution:

$$\frac{N_{ToFH}}{\sum Events\ with\ FastRPC\ Hits} = A_0 \cdot e^{\left(-\frac{t}{\tau_0}\right)} + A_1 \cdot e^{\left(-\frac{t}{\tau_1}\right)} + A_2 \cdot e^{\left(-\frac{t}{\tau_2}\right)} + c, \tag{4.1}$$

where N_{ToFH} is the number of first hits identified per fastRPC time bin (0.8 ns), τ_0, τ_1 and τ_2 are the

A_0	τ_0 (ns)	A_1	τ_1 (ns)
$3.75\times10^{-3}\pm1.50\times10^{-4}$	4.09 ± 0.13	$1.44\times10^{-4}\pm1.4\times10^{-5}$	33.0 ± 2.6

A_2	τ_2 (ns)	c
$1.82\times10^{-5}\pm8.2\times10^{-7}$	480 ± 28	$2.93\times10^{-6}\pm1.38\times10^{-7}$

Table 1: Fit parameters for the 80 GeV π^+ FastRPC data, using the fit function in equation 4.1.

A_0	τ_0 (ns)	A_1	τ_1 (ns)
$1.89\times10^{-2}\pm1.3\times10^{-3}$	4.58 ± 0.22	$2.01\times10^{-3}\pm2.8\times10^{-4}$	13.7 ± 10.6

A_2	τ_2 (ns)	c
$2.66\times10^{-5}\pm6.2\times10^{-7}$	566 ± 26	$4.46\times10^{-6}\pm2.22\times10^{-7}$

Table 2: Fit parameters for the 60 GeV π^+ T3B data, using the fit function in equation 4.1.

time constants of the short, intermediate and long components respectively and A_0, A_1 and A_2 are the corresponding amplitudes. The fit was performed in the time range of [4, 2000] ns, excluding the peak region of the prompt contributions. The resulting function is shown by the solid line in figure 5. Table 1 summarizes the obtained fit parameters.

5. Comparison to T3B

The comparison of results obtained with FastRPC and T3B provides the possibility to investigate the sensitivity of each of the readout media to the different time components in the hadronic cascade. The beam conditions are slightly different for the two experiments, since data for the 60 GeV energy point are shown for T3B, whereas FastRPC has data for 80 and 180 GeV. The results are still comparable since, as already shown in figure 5, the time spectra for FastRPC as well as for T3B [2] do not depend on the beam energy. Similarly, the geometry for the two experiments is similar but not identical. The same absorber structure is used in both cases, but the active elements are different, resulting in somewhat different material budgets. While the scintillator cassettes used in the WAHCAL have two 2 mm thick steel cover plates in addition to the 5 mm thick scintillator layer and a thin PCB, the RPC units in the WDHCAL have one 2 mm thick steel cover plate and one 2 mm thick copper cover plate, 1.9 mm of glass, a PCB and other thinner components. Since studies by T3B have also shown that the longitudinal dependence of the time structure is rather weak [2], these differences should not affect the validity of the comparison.

Time of First Hit Distribution

Differences are expected in particular for neutron-induced processes, since in the FastRPC gaseous detector the amount of hydrogen is much lower than in plastic scintillators. In addition, the low density of the gas further reduces the probability for neutron interactions in the active medium. To facilitate this comparison, the fit discussed above is also applied to the T3B data.

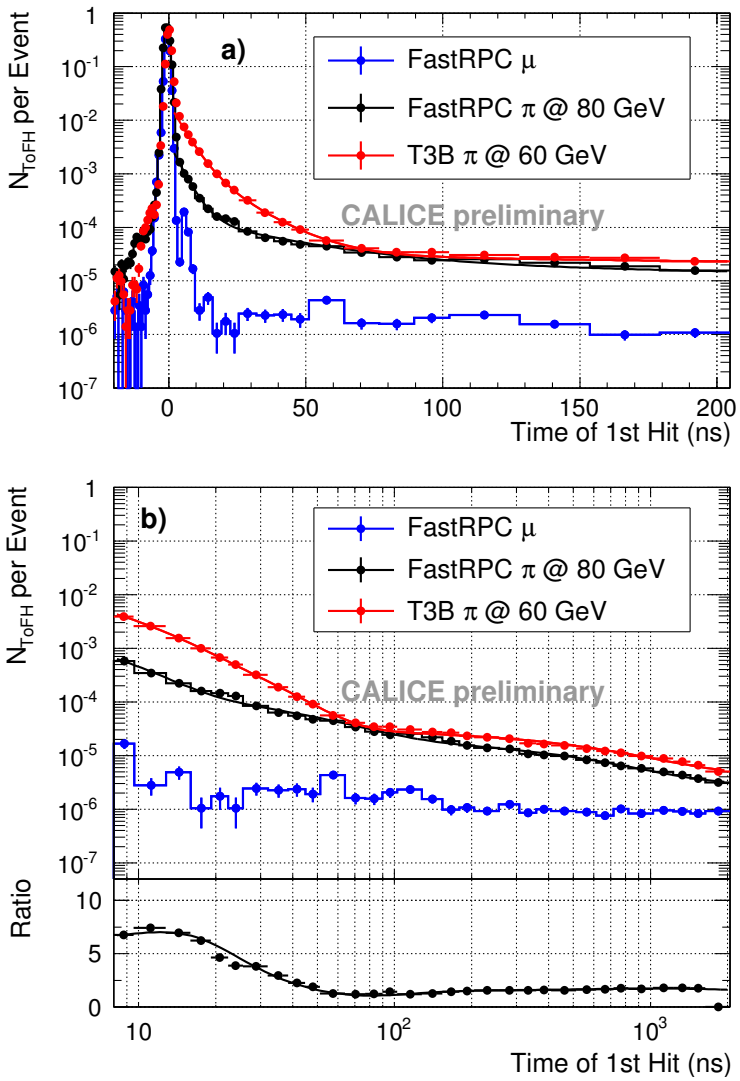

Figure 6: Comparison of the time of first hit distribution observed in FastRPC (80 GeV $\pi^{\pm}$) and T3B (60 GeV π^{+}), normalized to the number of events with at least one hit in the FastRPC and T3B detectors, respectively. Also shown are triple-exponential fits to the data, as discussed in the text. (a) A time window of [-20, 200] ns including the main prompt peak, and (b) a double logarithmic plot of the [8, 2000] ns, where the lower panel shows the ratio between histograms and between fits for the data of the two experiments.

Table 2 summarizes the results of the fit of equation 4.1, applied to 60 GeV π^{+} T3B data. Figure 6 shows a superposition of the results of the T3B and the FastRPC experiments. The comparison shows that the intermediate component, which is expected to be dominated by neutron elastic scattering in the detector of MeV-scale spallation and evaporation neutrons, is highly suppressed in the gaseous detector. Figure 6 b) shows the ratio plot of both the data points over the full range with the exception of the instantaneous peak region, as well as the fitted function for the two experiments. The curve shows a discrepancy up to a factor of eight in the intermediate region, that

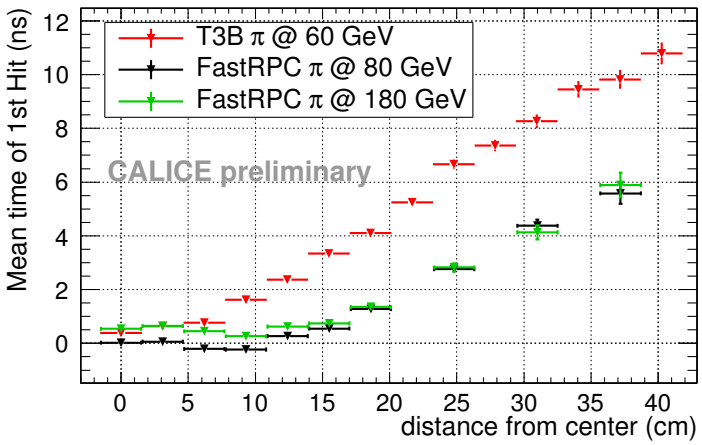

Figure 7: Mean time of first hit, calculated over the [-20, 200] ns sampling window, as a function of the distance from the nominal beam axis for 80 and 180 GeV pions. The plot shows no substantial dependence on the particle energy for the FastRPC based detector.

lowers to a factor two for the very late component. The fact that there remains a discrepancy for the late time components might be due to contributions from several different neutron processes: some of the metastable states produced in the absorber decay, emitting additional neutrons, nuclear fragments or photons over a long period of time. While both setups are sensitive to photons in the MeV range coming from nuclear de-excitation, the sensitivities are not expected to be equal due to the low density of the gas in the RPCs and the correspondingly reduced interaction probability for photons directly in the sensitive medium itself. This would qualitatively explain the discrepancy between FastRPC and T3B which is still present after 100 ns and more.

Radial Timing Profile

If we average the time of first hit for every channel in a time window from -20 to 200 ns and plot the mean as a function of the distance from the nominal beam axis, we obtain figure 7. This figure shows that the mean time of energy deposition depends on the distance from the beam axis. This behavior is expected since relativistic hadrons and electromagnetic subshowers, which contribute to the instantaneous part of the hadronic cascade, are more pronounced in the region close to the shower axis. Delayed components, which are often linked to neutrons, are more widely spread out over the calorimeter volume, and thus gain in relative importance at larger radii. No energy dependence of the distribution is observed, given the systematic uncertainties of the t = 0 determination of $\sim$200 ps.

The same analysis was also performed for T3B data, also shown in figure 7. The growth of the mean time of first hit with radius is more pronounced for scintillator readout. This effect is attributed to a larger contribution from late energy deposits in scintillator compared to RPCs, which are widely spread over the calorimeter volume.

6. Summary

FastRPC has studied the time structure of hadronic showers in tungsten with gaseous readout. It has demonstrated that an extended time structure is also visible with an RPC based detector, although to a lesser degree in comparison to plastic scintillators. The time distribution of energy depositions is characterized by three different time constants, consistent with the expectation of a prompt contribution from relativistic particles, a neutron component on the few 10 ns level and a long contribution from neutron-induced and other nuclear processes. In the energy range from 80 GeV to 180 GeV, no energy dependence of the measured time structure has been observed.

The direct comparison with T3B data shows a suppression of the intermediate time component by a factor of seven to eight in the range of 10 ns to 20 ns, and a factor of four up to 30 ns. Since the hydrogen content of the T3B plastic scintillators is substantially higher than that of the RPC detectors, this observation confirms the link of this shower component to neutron elastic scattering. This different sensitivity to some aspects of the hadronic cascade is also reflected in a difference of the radial dependence of the average time of first hit, which increases more strongly towards large radii for scintillator readout than for gaseous active media.

Acknowledgements

The research leading to these results has received funding from the European Commission under the FP7 Research Infrastructures project AIDA, grant agreement no. 262025 and by the DFG Cluster of Excellence "Origin and Structure of the Universe".

References

[1] P. Lebrun, L. Linssen, A. Lucaci-Timoce, D. Schulte, F. Simon, *et. al.*, *The CLIC Programme: Towards a Staged e^+e^- Linear Collider Exploring the Terascale : CLIC Conceptual Design Report*, arXiv:1209.2543.

[2] CALICE Collaboration, *The Time Structure of Hadronic Showers in Tungsten and Steel with T3B*, *CALICE Analysis Note CAN-038 (2012)*.

[3] CALICE Collaboration, *Analysis of Tungsten-DHCAL Data from the CERN Test Beam*, *CALICE Analysis Note CAN-039 (2012)*.

[4] M. Szalay, *Study of hadronic showers with the fastRPC analog readout*, Master's thesis, Technische Universität München, 2013.